IOPscience iopscience.iop.org

Home Search Collections Journals About Contact us My IOPscience

Linearity Characteristics of Field-Plated AlGaN/GaN High Electron Mobility Transistors for Microwave Applications

This content has been downloaded from IOPscience. Please scroll down to see the full text.

2010 Jpn. J. Appl. Phys. 49 014103

(http://iopscience.iop.org/1347-4065/49/1R/014103)

View the table of contents for this issue, or go to the journal homepage for more

Download details:

IP Address: 140.113.38.11
This content was downloaded on 25/04/2014 at 06:07

Please note that terms and conditions apply.

Linearity Characteristics of Field-Plated AlGaN/GaN High Electron Mobility Transistors for Microwave Applications

Jui-Chien Huang, Heng-Tung Hsu[1], Edward-Yi Chang*, Chung-Yu Lu,
Chia-Ta Chang, Fang-Yao Kuo[1], Yi-Chung Chen, and Ting-Hung Hsu

Department of Materials Science and Engineering, National Chiao-Tung University, Hsinchu, Taiwan 30010, R.O.C.
[1]*Department of Communications Engineering and Communication Research Center, Yuan Ze University, Chunli, Taiwan 32003, R.O.C.*

Received July 24, 2009; accepted October 6, 2009; published online January 20, 2010

A field-plated (FP) AlGaN/GaN high electron mobility transistor (HEMT) was fabricated. Investigations on the linearity characteristics were performed through two-tone and wide band code division multiple access (WCDMA) modulated excitations. The FP-HEMT exhibited an improved breakdown voltage of 160 V compared with that of the conventional HEMT. Additionally, a higher output power of 25.4 dBm with 43% power added efficiency at a 30 V drain bias at 2 GHz was achieved. When biased at 30 V and 15 mA/mm current density, the third-order intermodulation (IM3) level was measured to be −27.1 dBc (at P_{1dB}) and the adjacent channel power rejection (ACPR) was −33.8 dBc (at P_{1dB}) under WCDMA modulation at 2 GHz. Measurement results revealed that the field-plated structure improved the linearity performance over the conventional structure at high output power levels even beyond P_{1dB}. © 2010 The Japan Society of Applied Physics

DOI: 10.1143/JJAP.49.014103

1. Introduction

Modern wireless communication systems have put extremely stringent requirements on both the power and linearity performance of power amplifiers for base stations operating at microwave frequencies. Silicon laterally diffused metal oxide semiconductor (LDMOS) power transistors have been dominant for such applications over the years. However, with the approaching limits of operability for such devices, there will be a need for other semiconductor materials to fulfill the high-power and high-linearity requirements of the next generation wireless technology. Gallium nitride (GaN) has been acknowledged as a prime candidate for high-power microwave applications owing to their high breakdown field (3 MV/cm), high electron saturation velocity (2.5×10^7 $cm^2 V^{-1} s^{-1}$), and high operating temperature.[1)] The associated AlGaN/GaN high electron mobility transistor (HEMT) structure further features relatively high electron mobility due to the existence of two-dimensional electron gases (2DEGs). Such superior electronic properties of the structure have generated record-high output power densities at S- and X-bands.[2,3)]

Recently, a field plate structure has been widely used in AlGaN/GaN HEMTs for power application. It was believed that the field plate cannot only enhance breakdown voltage but also suppress the surface state, which markedly affected the power performance of GaN HEMTs.[4,5)] The effects of insulator thickness and geometry of the field plate on breakdown voltage and frequency response were discussed.[4,6,7)] Meanwhile, the extension gate of the field plate increases the gate capacitance (C_{gd}) and results in degraded transconductance and gain characteristics. While studies have been focused on the effect of field plates to increase the breakdown voltage, not much research effort has been devoted to the linearity performance of the field-plated (FP) AlGaN/GaN HEMT.[7,8)] Thus, the main focus of this study is the investigation of the linearity characteristics of an FP-HEMT under different bias conditions.

2. Experimental Methods

The AlGaN/GaN HEMT epitaxy structure in this study was grown on sapphire by metal organic chemical vapor deposition. The structure included 3-μm-thick undoped GaN buffer and 30-nm-thick undoped $Al_{0.25}Ga_{0.75}N$ layers. The Hall mobility and sheet carrier concentration were 1300 $cm^2 V^{-1} s^{-1}$ and 1×10^{13} cm^{-2}, respectively. Figure 1 shows a schematic cross section of the field-plated AlGaN/GaN HEMT. Mesa etching was performed by ICP-RIE with a Cl_2/BCl_3 gas mixture. Ohmic alloy Ti/Al/Ni/Au was deposited by e-beam evaporation and annealed in nitrogen atmosphere at 800 °C for 60 s. The spacing between source and drain was 7 μm. The ohmic contact resistance was 3×10^{-6} Ω cm^2. After ohmic formation, the sample was dipped in dilute HCl for 1 min for cleaning. After cleaning, a Ni/Au gate ($L_g = 1$ μm) was deposited and subsequently the device was passivated with a 100-nm-thick SiN_x layer grown by plasma-enhanced chemical vapor deposition. Finally, Ti/Au was deposited as the field plate structure ($L_{FP} = 1$ μm), which was connected to the gate electrode. The device was 100 μm FET with gate finger widths of 50 μm. In this study, both FP and non-FP (nFP) AlGaN/GaN HEMTs were fabricated to observe the effect of the field plate structure on the linearity characteristics for microwave applications.

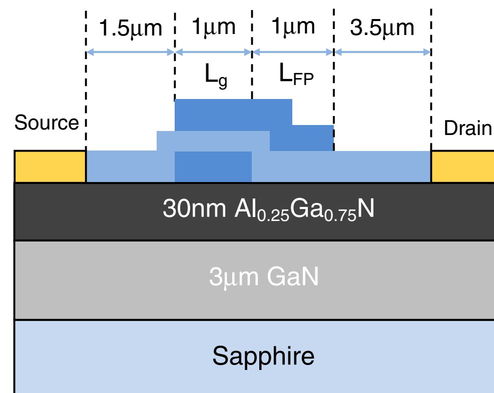

Fig. 1. (Color online) Schematic cross section of the field-plated AlGaN/GaN HEMT with 2-μm-long Ti/Au deposited as the field plate.

*E-mail address: edc@mail.nctu.edu.tw

 © 2010 The Japan Society of Applied Physics

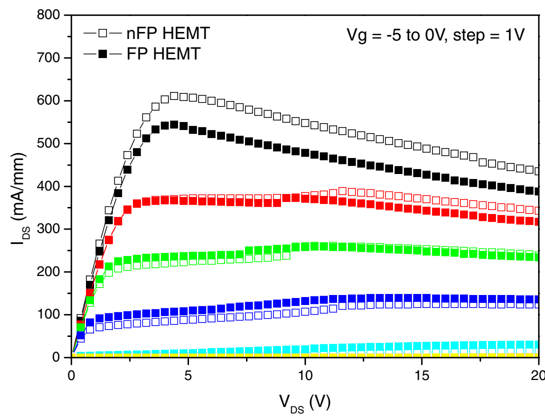

Fig. 2. (Color online) DC *I*–*V* curves of FP-HEMT and nFP-HEMT.

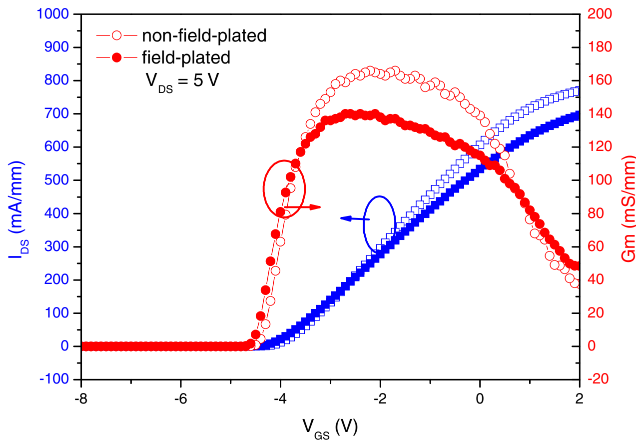

Fig. 3. (Color online) Comparison of transconductance curves for nFP-HEMT and FP-HEMT.

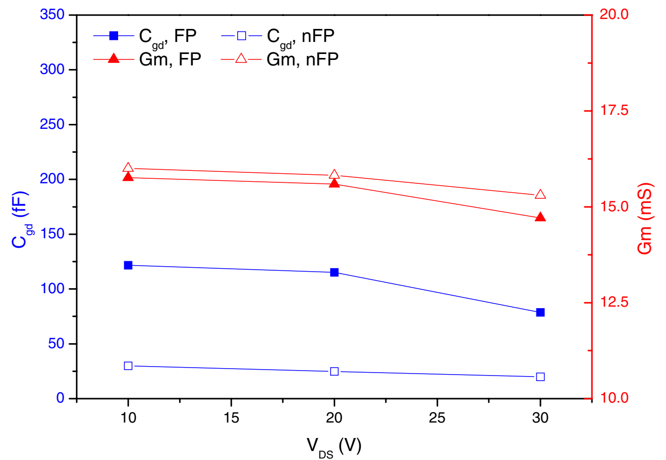

Fig. 4. (Color online) Dependence of equivalent model parameters on drain bias for FP and nFP devices.

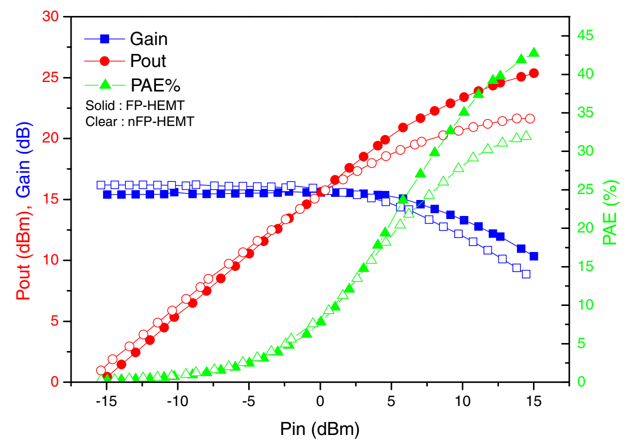

Fig. 5. (Color online) Power performance of FP-HEMT and nFP-HEMT at 2 GHz.

3. Results and Discussion

3.1 DC characteristics

Figures 2 and 3 show the DC characteristics of FP and nFP AlGaN/GaN HEMTs. For the nFP-HEMT, the maximum drain current at $V_{GS} = 0$ was 610 mA/mm and the maximum transconductance was 160 mS/mm, compared to those of 545 mA/mm and 140 mS/mm for the FP HEMT, respectively. The reduction of saturation drain current in the FP-HEMT is due to the gate extension from the field plate structure. Additionally, the thickness of the SiN_x passivation layer was only 100 nm. These two factors make the effective gate length larger and decrease the saturation drain current. However, with the field plate structure, the FP-HEMT exhibited an improved breakdown voltage of 160 V compared with 90 V for the nFP-HEMT, implying that a higher drain bias can be applied for higher output power and better linearity.

3.2 Small signal characteristics

S-parameters of the 100 µm FP and nFP-HEMT devices were measured from 1 to 40 GHz using a Cascade Microtech on-wafer probing system with an HP8510XF vector network analyzer. Additionally, a standard load-reflection-reflection-match (LRRM) calibration method was used to calibrate the measurement system, and the calibrated reference planes were at the tips of the corresponding probes. The parasitic effects (mainly capacitive) from the probing pads have been carefully removed from the measured *S*-parameters using the same method as Yamashita *et al.* and the equivalent circuit model reported by Dambrine *et al.*[9,10] Figure 4 shows the extracted parameters as functions of drain voltage for both devices. As is observed, the major impact of the field plate on the device is the increase in the drain-to-gate capacitance (C_{gd}). This increase acted as negative feedback from the drain to the gate and would have certain effects on the linearity performance due to the amount of frequency-dependent feedback provided. Meanwhile, a slight reduction in RF Gm for the device with the field plate was also observed. With the reduction in RF Gm and increase in C_{gd} for the FP device, the extracted current gain cutoff frequency (f_T) was 8.8 GHz, compared with 9.4 GHz for the nFP device.

3.3 RF power performance

The power performance was measured using a FOCUS on-wafer load–pull system. The devices were tuned for the maximum output power. Figure 5 shows the output power, gain, and PAE as a function of input power for both devices at 2 GHz when biased at 30 V with a 15 mA/mm current density. The optimum load reflection coefficients were

 © 2010 The Japan Society of Applied Physics

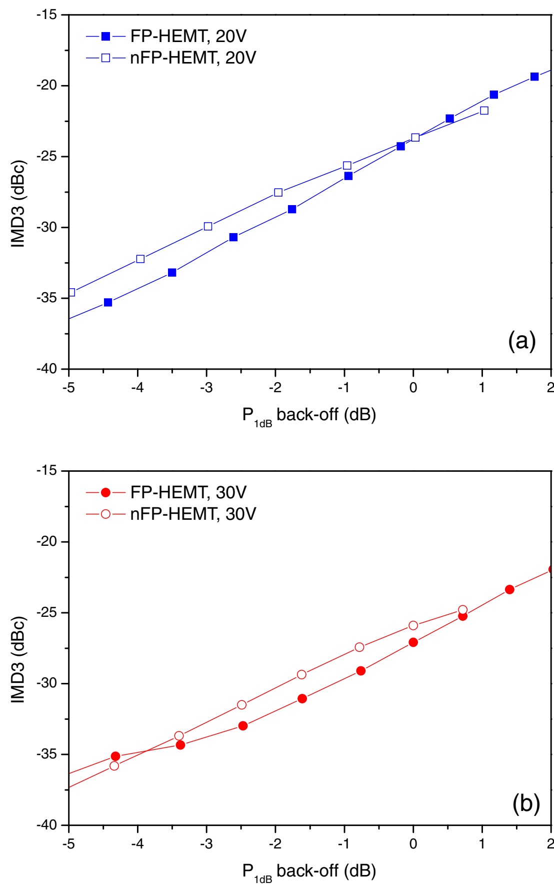

Fig. 6. (Color online) Third-order IMD versus power back-off from P_{1dB} for FP-HEMT and nFP-HEMT, (a) $V_{ds} = 20$ V and (b) $V_{ds} = 30$ V.

$\Gamma_{opt} = 0.886\angle 9.9°$ and $0.885\angle 7.5°$ for FP and nFP devices, respectively. A higher output power of 25.36 dBm and PAE of 43% were achieved for the FP device. Meanwhile, P_{1dB} for the FP and nFP devices when biased at a 30 V drain bias were 18.52 and 16.26 dBm, respectively. The softer gain compression of the FP device is believed to be the reason for the linearity improvement at high output power levels even beyond P_{1dB}. Such superior performance is mainly attributed to the reduction of trapping in surface states due to the field plate structure.[4)]

3.4 Linearity measurements

For linearity characterization, both two-tone and digitally modulated WCDMA signals were used as excitation for third-order intermodulation distortion (IMD3) and adjacent channel power ratio (ACPR) measurement, respectively. The load impedances were set at maximum output power for both measurements. The two carriers were set at a center frequency of 2 GHz with 1 MHz apart for IMD3 measurement. Figures 6(a) and 6(b) show the measured IMD3 as a function of power back-off from P_{1dB} biased at $V_{DS} = 20$ and 30 V with a 15 mA/mm current density for the FP and nFP devices. It is clear that both devices exhibited comparable performance with slight improvement observed for the FP device. This improvement in IMD3 is related to the soft gain compression of the FP device caused by the field plate. Generally, soft gain compression tends to suppress the AM–AM distortion at the same output power level. Thus, the reduction of surface state trapping through the application of the field plate will result in soft gain compression and thus better IMD3 performance as observed from the measurement.

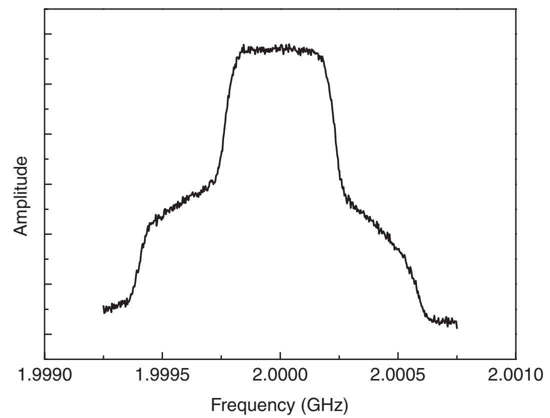

Fig. 7. Spectral regrowth plot for FP device under WCDMA modulation.

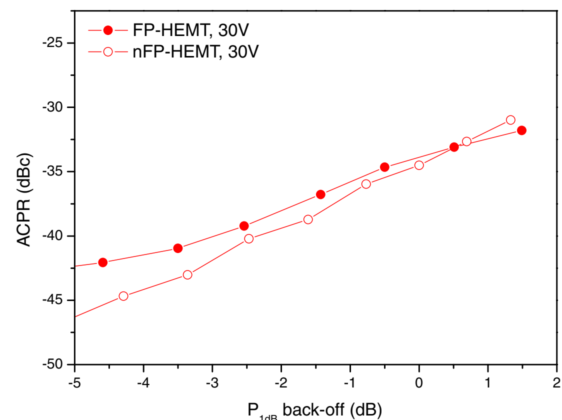

Fig. 8. (Color online) WCDMA ACPR data versus power back-off from P_{1dB} for FP-HEMT and nFP-HEMT.

To further characterize the device performance under digitally modulated excitation, we used a wide band code division multiple access (WCDMA) signal as the input. The bandwidth of integration was 3.84 MHz and the center spacing of the adjacent passband was 5 MHz as defined for the WCDMA system. Figure 7 shows the spectral regrowth plot for the FP device at 2 GHz when biased at 30 V with a corresponding output power at P_{1dB}. An ACPR of -33.8 dBc was achieved. Figure 8 shows the ACPR comparison for the FP and nFP devices as a function of power back-off from P_{1dB} biased at $V_{DS} = 30$ V with a 15 mA/mm current density. Again, the load impedances were set to be the same as those in the case for IMD3 measurement. It was observed that the FP device exhibited a better ACPR performance at and beyond P_{1dB} than the nFP device. This improvement makes the FP device favorable for operation under higher output power.

4. Conclusions

In this study, a field-plated AlGaN/GaN HEMT device has been fabricated and characterized. Measurement results revealed an output power of 25.36 dBm with a linear gain of 15.39 dB achieved for the FP-HEMT at 2 GHz when biased at $V_{ds} = 30$ V. An improvement in breakdown

© 2010 The Japan Society of Applied Physics

voltage from 90 to 160 V was observed. The measured IMD3 and ACPR for the FP device both showed better linearity than those for the nFP device at high output power levels even beyond P_{1dB}. The improvement in linearity is related to the soft gain compression of the FP structure due to the feedback provided by the field plate. Such improvement makes FP devices favorable for operation under higher output power conditions.

Acknowledgments

The authors would like to acknowledge the support from the National Science Council and the Ministry of Economic Affairs, Taiwan, R.O.C., under the contracts: NSC 97-2221-E-009-156 and NSC 97-2221-E-155-070.

1) W. Nagy, J. Brown, R. Borges, and S. Singhal: IEEE Trans. Microwave Theory Tech. **51** (2003) 660.
2) Y. Ando, Y. Okamoto, H. Miyamoto, T. Nakayama, T. Inoue, and M. Kuzuhara: IEEE Electron Device Lett. **24** (2003) 289.
3) R. Chu, L. Shen, N. Fichtenbaum, D. Brown, Z. Chen, S. Keller, S. P. DenBaars, and U. K. Mishra: IEEE Electron Device Lett. **29** (2008) 974.
4) Y.-F. Wu, A. Saxler, M. Moore, R. P. Smith, S. Sheppard, P. M. Chavarkar, T. Wisleder, U. K. Mishra, and P. Parikh: IEEE Electron Device Lett. **25** (2004) 117.
5) Y. Okamoto, Y. Ando, K. Hataya, T. Nakayama, H. Miyamoto, T. Inoue, M. Senda, K. Hirata, M. Kosaki, N. Shibata, and M. Kuzuhara: IEEE Trans. Microwave Theory Tech. **52** (2004) 2536.
6) S. Karmalkar and U. K. Mishra: IEEE Trans. Electron Devices **48** (2001) 1515.
7) H. Xing, Y. Dora, A. Chini, S. Heikman, S. Keller, and U. K. Mishra: IEEE Electron Device Lett. **25** (2004) 161.
8) Y. Dora, A. Chakraborty, L. McCarthy, S. Keller, S. DenBarrs, and U. K. Mishra: IEEE Electron Device Lett. **27** (2006) 713.
9) Y. Yamashita, A. Endoh, K. Shinohara, M. Higashiwaki, K. Hikosaka, T. Mimura, S. Hiyamizu, and T. Matsui: IEEE Electron Device Lett. **22** (2001) 367.
10) G. Dambrine, A. Cappy, F. Heliodore, and E. Playez: IEEE Trans. Microwave Theory Tech. **36** (1988) 1151.

© 2010 The Japan Society of Applied Physics